Available online at www.sciencedirect.com
ScienceDirect
Advances in Space Research 39 (2007) 627–635
ADVANCES IN SPACE RESEARCH (a COSPAR publication)
www.elsevier.com/locate/asr

Global scale lunar sample return using projectiles launched from a low-flying spacecraft

Ian Garrick-Bethell *, Erwan Mazarico, Wesley Andrés Watters

Massachusetts Institute of Technology, Department of Earth, Atmospheric and Planetary Sciences, 54-520, 77 Massachusetts Avenue, Cambridge, MA 02139, USA

Received 12 May 2006; received in revised form 14 October 2006; accepted 19 October 2006

Abstract

Since the Moon has no atmosphere it is possible to fly over the surface at very low altitudes without experiencing drag forces. If a spacecraft flying at a low altitude were to fire a projectile into the lunar surface, a second trailing spacecraft could capture material from the resulting cloud of ejecta. This procedure could be repeated over many sites on the Moon with a fresh collector for each location. Eventually, the collector spacecraft would seal its cargo in a reentry vehicle and return to Earth with the samples. Compared with a robotic lander, the advantage of this architecture is the ability to sample locations over the entire Moon, wherever the topography will permit such maneuvers. Our crater ejecta models show that 1–10 g of material can be collected from the ejecta curtain of a 2 m radius crater at an altitude of 150 m, assuming a collector surface area of 1 square meter. We studied numerous means of creating these craters and developed two scenarios: a reduced velocity explosive excavator (EE), and a higher velocity impact excavator (IE).

Keywords: Moon; Impactor; Sample return; Ejecta

1. Introduction

1.1. Concept background

The recently successful NASA Deep Impact mission used a copper projectile to reveal the interior of the comet Tempel-1 (A'Hearn et al., 2005). The NASA Stardust mission recently flew by the comet Wild-2 and successfully collected small particles in the coma (Brownlee et al., 2006). In our mission concept we combine these two missions: we use an orbiting spacecraft to launch an artificial projectile towards the Moon to create a cloud of ejecta, which we capture with a second spacecraft flying very low above the surface. The collector spacecraft returns to a higher, safer parking orbit after sample collection. The major advantage of this architecture is that the process can be repeated at unique locations all over the Moon with a fresh collector for each site. After conceiving this mission concept we found related concepts for Mars (Walker et al., 2004) and its satellites (Pieters et al., 1999), but not for the Moon. Since low altitude flight represents the greatest difficulty in our mission, improved topography and gravity from the upcoming NASA Lunar Reconnaissance Orbiter will be important in making this mission feasible (Smith and Zuber, 2005). Around the time of completion of our study, NASA announced a precision impactor mission to the lunar poles, suggesting our mission concept may not be too far away in terms of technology. The goal of this paper is to present some of the major issues associated with our mission.

1.2. Example target: lunar far side volcanic materials

Our baseline objective will be to sample basaltic regolith and tiny pyroclastic glasses from multiple mare locations on the lunar far side. Example targets include mare Moscoviense, mare within the crater Tsiolkovsky, and mare

* Corresponding author. Tel.: +1 646 206 2830.
E-mail address: iang@mit.edu (I. Garrick-Bethell).

0273-1177/$30 © 2007 Published by Elsevier Ltd on behalf of COSPAR.
doi:10.1016/j.asr.2006.10.010

inside the South Pole-Aitken basin (SP-A), including mare Ingenii, mare in the crater Leibnitz, mare in the Poincaré basin, and mare in the Apollo basin. To illustrate our concept, we will specifically examine sampling material from the central mare of the Apollo basin. Sampling material from anywhere on the far side of the Moon would provide insight into the major geochemical and geologic dichotomies between the far side and near side. Some questions we seek to answer include, why is the near side enriched in thorium and other heat-producing elements, and why is volcanism limited primarily to the near side? Additionally, are some SP-A mare deposits truly devoid of thorium as orbital measurements imply (Hagerty et al., 2006a), and what are the implications for the differentiation of the far side? We note that pyroclastic glasses offer a particularly unique view of the deep interior, and are likely the closest approximation to a primary mantle melt (Delano, 1986). Do far side volcanic glasses contain similar radioactive element and volatile concentrations as those on the near side? Also, what was the timing of the far side volcanic events, and did it coincide with any major near side volcanism? Are there large differences in titanium, iron, and aluminum content in far side basalts, and can these materials be linked to similar basalt groupings on the near side? How do inferences from remote sensing of the far side compare with results from actual samples? Lastly, the relatively smooth topography of mare terrain may make the sampling process less risky.

How much material should be collected? The Stardust mission returned on the order of 1 mg of material from the comet Wild-2, but lunar science objectives require more material. One past SP-A sample return study proposed ~1 kg of regolith fragments >2 mm (Jolliff et al., 2003), and Duke (2003) suggested 750 g of coarse fines (2–4 mm) and 250 g of bulk regolith. During the 1970s three robotic Soviet missions returned sample cores of 30, 101, and 170 g. We will explore the possibility of collecting up to 10 g of regolith per site, using a 1 m^2 collector. Using the regolith grain distribution from Apollo 17 mare soil 71061, 1 (“a typical Apollo 17 mare regolith” (Heiken, 1975)), a grain density of 2800 kg/m^3, and the mean 1×3 prolate ellipsoid volume for each grain size bin (Heywood, 1971), 10 g of bulk material yields over 10,000 fragments 100–250 μm in diameter, about 2000 fragments 250–500 μm in diameter, about 130 fragments 500–1000 μm in diameter, and about 25 fragments greater than 1 mm. Of the grains greater than 250 μm in 71061, 1, about half were identifiable as equigranular basaltic rocks (Heiken, 1975). No large pyroclastic deposits have been remotely identified in the Apollo basin central mare (Gaddis et al., 2003), but it is likely that some pyroclastic glasses would be present, since such glasses were identified at all Apollo sites (Delano, 1986). We assume that the grain size distribution below ~2 mm remains constant during the crater excavation and ejection process, since we have not found data in the literature that would suggest otherwise.

It can be difficult to determine the petrology of lunar rocks smaller than about 250 μm, a value which depends on the characteristic size of crystals in the rock (Heiken et al., 1991). However, as reviewed in chapter 7 of Heiken et al. (1991), insights into the basement rock type can be made using mostly monomineralic fragments (Bence and Papike, 1972; Smith, 1974; Smith and Steele, 1974; Steele and Smith, 1976; Vaniman et al., 1979). This type of analysis could supplement the results obtained from the larger grain size fractions returned. Determination of petrology and geochemistry has been achieved for lithic (rock) fragments smaller than 250 μm (Ma et al., 1978; Coish and Taylor, 1978), and in the range of 250–500 μm (Taylor et al., 1978). Geochemistry of pyroclastic spherules (~200 μm) continues to return insights into the composition of the lunar mantle (Hagerty et al., 2006b). As for geochronology, both small fragments of rock (~1 mg) (Burgess and Turner, 1998; Cohen et al., 2001), and ~200 μm glass spherules (Culler et al., 2000), can be dated using the $^{40}Ar/^{39}Ar$ technique (assuming sufficient native potassium). In sum, while it may be more difficult to obtain meaningful results from small rock samples, it is not impossible. Shearer and Borg (2006) have recently advocated the benefits of using small samples to study the Moon. We are encouraged by the 30 years of instrument development and general advancements in lunar science since most of the work on lunar soils.

1.3. Global scale sample return

The interior highlands terrain of SP-A is a valuable sample target for geochemistry and geochronology of the SP-A basin. A few other locations that could benefit from a small, limited sample, include the high-thorium Hansteen Alpha region (Lawrence et al., 2005), the thorium anomalies east of mare Ingenii (Garrick-Bethell and Zuber, 2005), the widespread low albedo swirls on mare surfaces, and the Aristarchus plateau. An ambitious, single mission to all of the above targets, including far side basalts, could provide a diverse global-scale dataset. In the future, water or hydrogen may be sampled on the lunar poles, albeit with the increased complexity of sampling a cloud of volatile material.

2. Crater ejecta models

2.1. Ejecta production model A

We must first estimate the amount of solid material ejected from a small crater produced by an impactor. The evolution of this material as a function of time and height will determine our orbit and maneuvering requirements. For a gravity dominated excavation process, which is the case for lunar regolith, the volume of ejecta V with a velocity of ejection v_e greater than a specified velocity v, can be written

$$V(v_e > v) = 0.32R^3\left(v/\sqrt{gR}\right)^{-1.22}, \quad (1a)$$

where R is the final crater radius, and $g = -1.62$ m/s^2 is the lunar gravitational acceleration (Housen et al., 1983; Melosh, 1989). Eq. (1a) is derived from explosion crater data (Andrews, 1975), and closely approximates experimental projectile data (Stöffler et al., 1975) and first-principles based numerical studies (Wada et al., 2006). The equation is valid for $0.6 < v/\sqrt{gR} < 10$. As we will mostly be interested in material for which $10 \leqslant v/\sqrt{gR} < 40$, we derive a similar function valid for this region using data from simulations of Wada et al. (2006),

$$V(v_e > v) = 6.0R^3\left(v/\sqrt{gR}\right)^{-2.45}. \quad (1b)$$

Due to uncertainties in modeling the impact process at higher velocities, Eq. (1b) may be less accurate than Eq. (1a), perhaps by a factor of two. Eqs. (1a) and (1b) are the basis of ejecta production model A.

We will calculate the amount of material in a 1-m-tall layer in the ejecta curtain at a given height h in the z-axis, at a given time t, Fig. 1. We then calculate the two vertical velocities that will deliver material to the top and bottom of the layer, for any given t, using $z = v_{e,z}t + \frac{1}{2}gt^2$, where $v_{e,z}$ is the vertical velocity component of the ejecta,

$$v_{e,z,\text{bottom}} = \frac{1}{t}\left(h - \frac{1}{2}gt^2\right) \quad (2a)$$

$$v_{e,z,\text{top}} = \frac{1}{t}\left((h + 1\text{ m}) - \frac{1}{2}gt^2\right). \quad (2b)$$

Assuming the mean ejection angle is 45° (Anderson et al., 2003; Melosh, 1989), we multiply Eq. (2) by $\sqrt{2}$ and obtain the maximum and minimum net velocities, $v_{e,\text{top}}$ and $v_{e,\text{bottom}}$. The volume of material ejected between the top and bottom of the 1-m layer is then given by Eq. (1): $V_{\text{layer}} = V(v_{e,\text{bottom}}) - V(v_{e,\text{top}})$. The ejecta forms an expanding inverted cone, and the area density (kg/m^2) of the 1-m layer at height h in this cone is then

$$\sigma = \rho V_{\text{layer}}/(\pi D \times 1\text{ m}), \quad (3)$$

where ρ is regolith density, and D is the cone diameter $= 2(v_e/\sqrt{2})t$.

Repeating the above process for multiple times, heights, and crater radii, we produce Fig. 2 over the valid values of v_e, assuming a regolith density of 1800 kg/m^3 (Heiken et al., 1991). The spacecraft will fly rapidly through the 1-m layer, encountering both curtain walls, therefore we multiply σ by two. The minimum mass collected occurs when the spacecraft travels through the ejecta cone centerline (Eq. (3), Fig. 2), and the amount increases several fold as the spacecraft's path approaches the cone edge. Fig. 2 shows that with a 1 m^2 collector, intercepting a minimum of 1 g requires flying at 150 m, ~8 s after formation of a

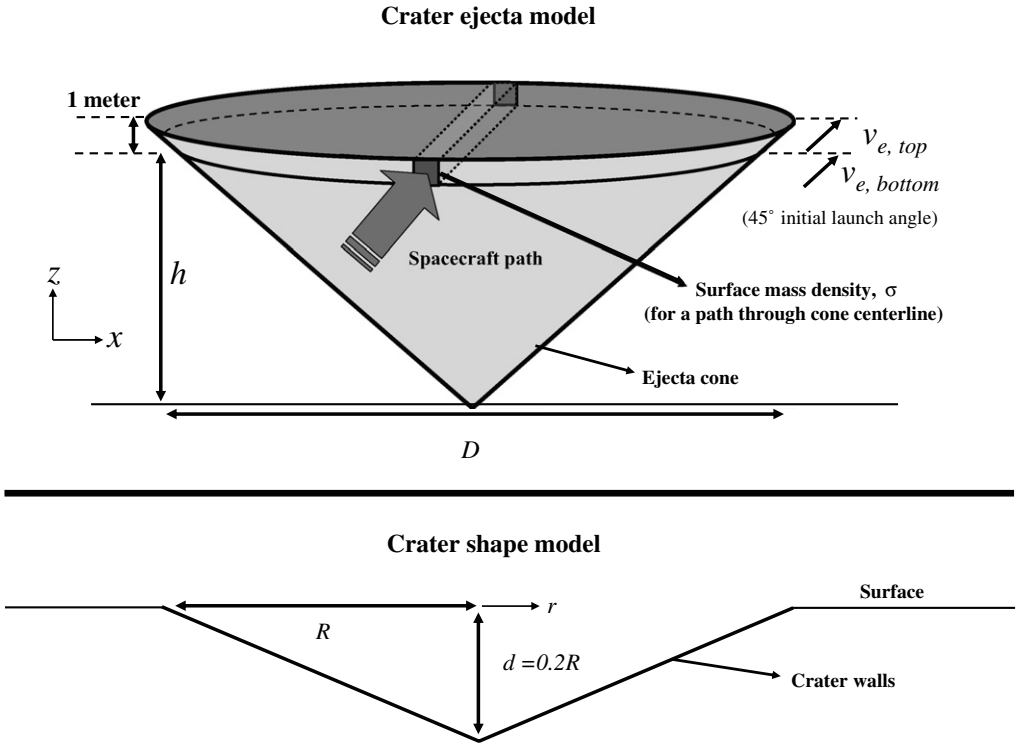

Fig. 1. Diagram showing parameters used in the crater ejecta models and crater shape model (not to scale). The ejecta of the crater forms an inverted expanding cone with an average initial ejection angle of 45°, but the instantaneous velocity vector of a given parcel of ejecta changes with time due to gravity. The spacecraft path through the cone centerline is shown intercepting the ejecta curtain twice.

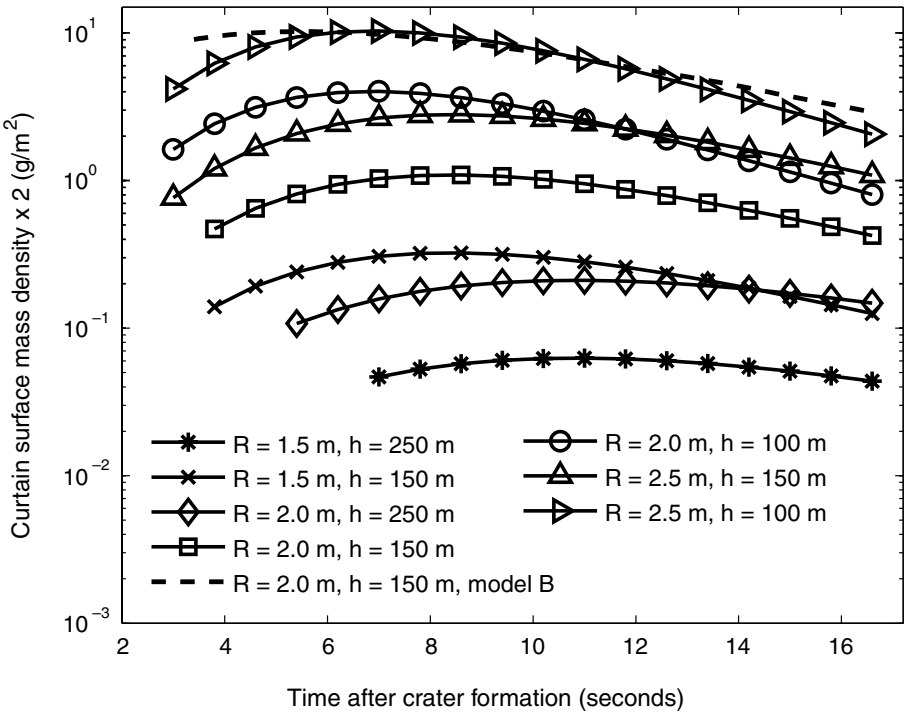

Fig. 2. Ejecta cone surface densities σ (g/m^2) from model A for various heights h and crater radius R (Eq. (3)), multiplied by two to account for the collector passing through the curtain twice. A 1 m^2 collector will intercept these amounts if it passes exactly through the cone centerline, but will collect more if it intercepts material nearer the curtain edge. In the flat portion of the right side of the curve, the function inflects when the rain-out of higher ejecta starts to contribute to the surface density. Also plotted are results from model B for the case $h = 150$ m, $R = 2$ m.

2 m radius crater. Cone diameter at this height and time is 380 m.

2.2. Ejecta production model B

Alternatively, according to an approach that we shall call model B, the ejecta curtain density can be estimated by calculating the expansion of a cylindrical shell of material initially inside the unexcavated crater, and following its evolution during excavation and flight. We start with a well known result from π-group scaling,

$$v_e = \beta\left(\frac{r}{R}\right)^{-\gamma}\sqrt{gR}, \tag{4}$$

where v_e corresponds to the velocity of material excavated at a distance r from the crater center during crater growth (Housen et al., 1983), and $v_{e,z} = v_{e,x} = v_e/\sqrt{2}$ (again assuming a mean ejection angle of 45°). A fit to results by Piekutowski (1980), as derived by Housen et al. (1983), gives $\beta = 0.62$ and $\gamma = 2.55$ for sand. This dependence of ejection velocity upon r means that a vertical spreading occurs over time between particles initially located at different radial positions inside the crater. That is, suppose that material excavated from radius r will have been launched to a height z at time t, then material excavated from $r + \partial r$ will reach a height $z + \partial z$ instead (where ∂z would be negative for $\partial r > 0$). We may calculate this spreading Δz along the vertical direction by substituting Eq. (4) for $v_{e,z}$ in $z = v_{e,z}t + \frac{1}{2}gt^2$ and differentiating with respect to r. This gives:

$$\Delta z = \frac{\partial z}{\partial r}_{,\partial r>0} = \frac{1}{\sqrt{2}}\left(\frac{\gamma\beta}{R}\left(\frac{r}{R}\right)^{-(\gamma+1)}\sqrt{gR}\right)t. \tag{5a}$$

Spreading also occurs along the circumferential direction as the ejecta curtain expands. If $2\pi v_{e,x}t$ is the ejecta curtain circumference at time t, and $2\pi r$ is the circumference of a cylindrical shell of ejected material initially at radial position r, then the circumferential spreading Δs is given by the ratio of ejecta curtain and excavation radii,

$$\Delta s = \frac{v_{e,x}t}{r} = \left(\frac{\beta}{r}\left(\frac{r}{R}\right)^{-\gamma}\sqrt{gR}\right)t. \tag{5b}$$

Eqs. (5a) and (5b) give the net expansion or dilation over time of a cylindrical shell of material initially inside the unexcavated crater. While the excavation velocity is a function of radius and circumferential position, the model (and Eq. (4)) assume that it is constant with respect to depth inside the shell, and also that the entire excavation is instantaneous. Since Eq. (4) is only valid for r greater than $\sim 0.2R$, we are ignoring contributions to the density from material ejected in this part of the crater volume (i.e., the earliest times). We also assume that the excavated volume from $0.2R$ to $0.3R$ (where the majority of material sampled at 150 m originates) is approximately cylindrical in shape (i.e., has a flat bottom).

The volume and circumferential area of infinitesimally thin cylindrical shells (of yet unexcavated crater material) increases as a linear function of radius. Therefore, the surface mass density of each cylindrical shell is constant with respect to r, and is effectively equal to the bulk volumetric density (1800 kg/m^3) projected onto the cylinder's surface (1800 kg/m^2). For a shell of radius r, we calculate the time t_1 required to reach a given height h. We then use Eqs. (5a) and (5b) to calculate the dilation $\Delta z \Delta s$ at t_1. Finally, we divide the initial surface density (1800 kg/m^2) by $\Delta z \Delta s$ to obtain the surface density at height h, and then repeat this calculation for a range of shell radii (and times), as plotted in Fig. 2.

Generally, model B predicts values higher than model A by about a factor of ten; at $h = 150$ m with $R = 2$ m, we obtain 10 g at 5 s after multiplying by two (Fig. 2). For the remainder of the paper we assume $R = 2$ m, and $h = 150$ m, yielding a mass between 1 and 10 g at the ejecta-cone centerline. Higher masses can be obtained either by increasing the crater radius, or collecting the sample at a lower altitude. For example, to collect 10 g using the predictions of model A, one would use $R = 2.5$ m and $h = 100$ m (Fig. 2), or $R = 2.0$ and $h = 75$ m (not shown). Until experimental verifications of these results can be obtained, we stress that they are only approximations. It is because of this uncertainty that we chose to present two different models of ejecta curtain density.

2.3. Oblique impacts and the use of explosives

The speed of a satellite in a circular lunar orbit is approximately 1.7 km/s at altitudes between zero and 50 km. If projectiles are given small downwards velocities so that they impact the surface, the angle of impact will be low. Impacts between 20° and 45° from the horizontal create asymmetric ejecta curtains with less material uprange of the crater, creating what is known as a "forbidden zone" (Anderson et al., 2003; Gault and Wedekind, 1978; Melosh, 1989). Impacts below 20° start to show another forbidden zone developing downrange of the crater. The development of either of these forbidden zones could reduce collected mass along the crater centerline. Therefore, if we strive for at least a 45° impact we must impart a downwards velocity of 1.7 km/s on the projectile. To be conservative, for a 45° impact the spacecraft would have to pass through the limb of the ejecta curtain, where the ejecta would be concentrated. This requirement increases the chance of missing the ejecta curtain altogether, and also makes our ejecta model less applicable. In addition, the mass of the propellant required to obtain 1.7 km/s velocities (Δv) is substantial. The possibility of using oblique (20–45°) impacts should be examined more carefully in the future, but we will now turn to an alternative approach.

We can avoid the problem of asymmetric ejecta and high Δv by creating a crater with explosives buried in the regolith by an obliquely penetrating projectile. Generally, buried explosives produce craters with symmetric ejecta curtains similar to vertical-impact craters when the chemical energy of the explosive matches the kinetic energy of a projectile, provided that an appropriate burial depth is used (Oberbeck, 1971). We may estimate the energy, W, to produce a crater of radius R using

$$R = 0.125 \rho_p^{1/6} \rho_t^{-1/2} W^{0.29} \sin(\theta)^{1/3}, \quad (6)$$

where ρ is density, θ is the angle of impact from the horizontal (90° for this estimate) and t and p here refer to target and penetrator, respectively (Gault, 1974; Melosh, 1989). For $R = 2$ m, $\rho_p = 1820$ kg/m^3 (below), and $\rho_t = 1800$ kg/m^3, we obtain $W = 77.8$ MJ. The required 77.8 MJ can be provided by 12.3 kg of the explosive cyclotrimethylenetrinitramine (RDX), with density 1820 kg/m^3 and heat of explosion of 6.3 MJ/kg (Köhler et al., 2002).

We now estimate the required depth of burial and simultaneously obtain a second estimate of required explosive mass. Both crater radius and depth of burial for different explosion craters can be related by scaling by $W^{1/3}$, e.g. $(R/W^{1/3}) = (R_o/W_o^{1/3})$ (Melosh, 1989). For R_o and W_o, we take the smallest set of crater radii, $R_o \sim 1.1$ m, produced by 0.6-m-deep 3.6 kg TNT explosions in a playa lake (Vortman, 1969), providing explosive energy $W_o = 16.2$ MJ, assuming a TNT heat of explosion of 4.5 MJ/kg (Köhler et al., 2002). For a crater radius of $R = 2$ m, the above data and scaling relationships predict $W = 97$ MJ and a required depth of burial of 1.1 m. This energy amounts to 15.4 kg of RDX, which we average with the first estimate to obtain 13.9 kg, with a volume of 7.7 L. Since we chose a low reference density for Eq. (6), and used the smallest craters in Vortman (1969), this mass is probably conservative. In fact, applying the same rules to other explosion craters in Vortman (1969) usually overestimates the explosive mass.

Finally, we add that if our crater is instead due to the energy of an impact at 45° without explosives (IE scenario), from Eq. (6) we obtain a mass of 16.1 kg (1.8 L volume), assuming a copper projectile (à la Deep Impact (A'Hearn et al., 2005)) with density 8960 kg/m^3, and a velocity of 2.4 km/s ($\sqrt{2} \times 1.7$ km/s). We will keep the IE scenario in mind, but explore the explosive excavator (EE) more extensively since it involves less mass, and is a more intriguing problem.

2.4. Upper limit on impact velocity for the EE scenario

Objects that strike the surface near 1.7 km/s start to interact with the surface material as if it were strengthless and responding hydrodynamically (Anderson et al., 1999a). The surface material effectively provides a ram pressure on the projectile given by $P = \frac{1}{2}\rho_t v^2$. When these pressures exceed the yield strength of the projectile, Y, the projectile will erode or deform. If the explosive device is timed to burst after sufficient burial, it must survive penetration. If we assume a casing made of steel, $Y = 1$ GPa, we find a maxi-

mum penetration velocity of about $v = (2Y/\rho_t)^{1/2} = 1$ km/s. Experiments in concrete validate this prediction (Nelson, 2002). We could not find published soil penetration experiments at speeds near 1.7 km/s, but evidence of erosion in 2 km/s rod impacts in water (Anderson et al., 1999b) and the predictions from Anderson et al. (1999a) suggests 1.7 km/s is too high (their Figs. 14 and 15). Until further work we must assume a 1 km/s limit for the EE scenario, which will require a braking burn (see below).

3. Spacecraft orbits and maneuvering requirements

3.1. Tandem spacecraft

Since the spacecraft is moving rapidly at a very low altitude, it is difficult to shoot a projectile at the surface and still leave 4–10 s (Fig. 2) for the ejected material to rise up and reach the planned spacecraft altitude of 150 m (Section 2.3). Before ~4 s, the required ejecta velocities to reach spacecraft altitudes of 150 m are beyond the limits of validity of Eq. (1b), and ejecta mass would be very low. For the IE scenario, shooting very far in front of the spacecraft to achieve the necessary delay would make the oblique-impact problem worse (Section 2.3), and for the EE scenario, the impact velocity would exceed 1 km/s (Section 2.4). Therefore, we propose using two spacecraft in a coplanar tandem orbit: the leading spacecraft fires the projectile from a higher altitude and the trailing collector spacecraft passes through the ejecta curtain at 150 m. Collection timing is prescribed by the along-track spacecraft separation, allowing for arbitrary velocities to be imparted to the projectiles. The tandem spacecraft design also permits the leading higher-orbit launch spacecraft to radar scan for topography anomalies that may endanger the lower collector spacecraft.

3.2. EE scenario in the Apollo basin mare

We used a 4th order Runge–Kutta integrator to find optimal parameters for the EE scenario in the Apollo basin central mare, with a collection point at (36.0°S, 208.0°E), Fig. 3. We assumed instantaneous velocity changes, which is sufficient because the spacecraft only makes changes on the order of 20–50 m/s, and our example scenario in the Apollo basin illustrates what is perhaps the Moon's most challenging topography (0.25 pixel/degree data from Smith et al., 1997). Our best solution suggests launching an EE projectile backwards from a lead spacecraft at 5 km altitude, with velocity of 1000 m/s at an angle of 20° below the orbit tangent. Firing slightly downwards reduces the time spent in flight, minimizing the cross-track error of the projectile. The impactor lands with a velocity 27° from the horizontal at 835 m/s, after 30 s of flight, and traversing 23 km of

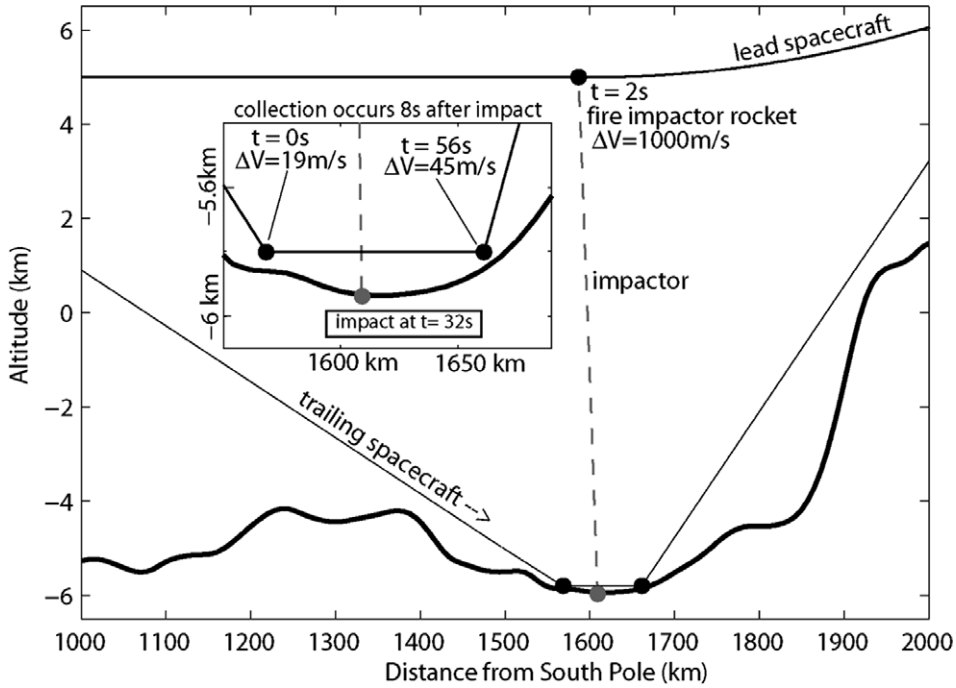

Fig. 3. Example of sample return from mare within the Apollo basin in the SP-A basin. The straight lines represent spacecraft trajectories, with the higher line representing the launch spacecraft. The backwards-launched EE scenario is shown (dashed line). A total Δv of 64 m/s is required for the collector spacecraft to enter and leave the low altitude sequence. The collector spacecraft spends 56 s over the mare, and all burns are idealized as instantaneous. Additional burns are required for both spacecraft to leave and return to their parking orbits (not shown, outside the figure bounds). Topography data are a transect across 208°E, with the collection point at (36.0°S, 208.0°E). The mare surface topography is not known to the level implied in the figure (see Section 3.3).

ground. At 27° steel projectiles with velocities near 800 m/s do not ricochet in soils (unpublished data, US Army, Aberdeen Proving Ground), although this value depends on the relative densities between the target and surface material. Assuming the EE scenario outlined above, at 27° a 1.1 m depth of burial requires moving through 2.4 m of regolith. This appears feasible given that penetration depths of ~6 m are achieved in soil at 300 m/s (Forrestal and Luk, 1992).

3.3. General orbit design, topography, and error

In both the IE and EE cases, both spacecraft descend from a high parking orbit to a lower approach altitude (Fig. 3). Based on simulations using GEODYN (Pavlis et al., 2006), a circular parking orbit altitude would have to be greater than about 25 km for the spacecraft to have a lifetime above 7 km altitude of more than 7 ± 4 days. For comparison, the Apollo 15 command module/lunar module pair used an elliptical descent orbit prior to the lunar module separation and landing. At descent orbit insertion, the paired spacecraft orbit had an initial apocenter altitude of 108 km, and a pericenter altitude of 17.6 km, which fell to 13.9 km after 12 h. In our mission, both spacecraft are brought from the parking orbit to a temporary 5 km altitude above the mean lunar radius. The lead spacecraft is brought to this low altitude to minimize the downward flight-time of the projectile, thereby reducing the projectile cross-track distance errors. Placing both spacecraft on the same temporary 5 km trajectory also allows some time for a final check of cross-track orbit drift.

During the 5 km approach the capture spacecraft is brought to the final altitude of 150 m just prior to the crater-forming event. The 150 m altitude is sustained for 56 s in this model, covering a distance of 95 km, which is about the diameter of the Apollo basin mare deposit. A 150 m rise over 95 km corresponds to a 0.1° slope. If the slope of the local terrain over 95 km is rising and is higher than 0.1°, a collision could occur. High-resolution topography is unavailable at Apollo, but Fig. 4 shows 13 laser shots from the Clementine laser altimeter (Smith et al., 1997), along longitude 207.0°E, from 35.5°S to 37.8°S. The radial errors are of the order 100 m, but even the slope from the lowest to the highest point, over 70 km, is only 0.1°. Short-wavelength topography anomalies will come primarily from raised crater rims, but surface images show most mare surfaces (including central Apollo) have ~100 km paths where there are no craters larger than ~2 km. Even craters of 4 km diameter have raised rims of only 150 m, based on scaling laws of Pike (1977). Finally, there are several other factors that can improve the success of such a low altitude flight: (1) fly-by times shorter than 56 s, (2) improved gravity and topography data from upcoming missions, (3) real time mapping of topography using the lead spacecraft, (4) collector spacecraft

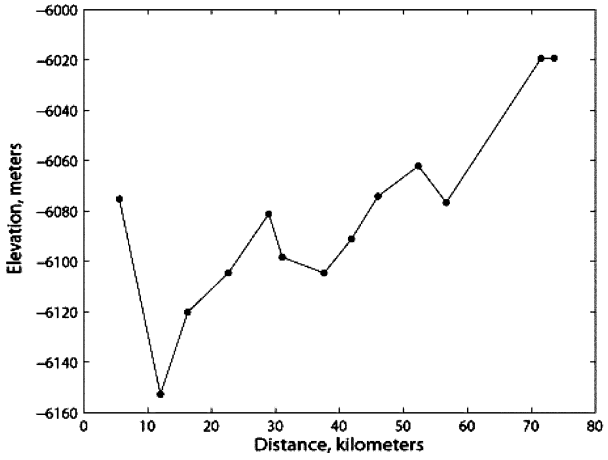

Fig. 4. Laser shots from the Clementine laser altimeter over the Apollo basin central mare. The shots were fired over longitude 207.0°E, from 37.7°S (leftmost point) to 35.5°S. The ordinate is the topographic elevation in meters, relative to the mean lunar radius of 1738 km.

ground-pointing radar that helps determine velocity corrections during the approach and fly-by.

To reduce the chance that cross-track errors will cause the trailing spacecraft to miss the ejecta curtain (~380 m wide at 8 s), two projectiles can be fired from the lead spacecraft at small and opposite angles from the vertical. The above EE scenario allows 1.0° in cross-track projectile launch error, assuming a double impact. If a known miss occurs, the leading spacecraft can be used as an extra projectile at the end of the mission. After sample collection both spacecraft must return to the parking orbit (~25 km) to avoid large gravity perturbations, and of course, topography. Fortunately, tandem spacecraft will experience similar gravity perturbations, minimizing their cross-track drift.

4. Mass and hardware design considerations

4.1. EE and IE penetrators

We estimate the penetrator rocket propellant mass, m_p, required for the EE scenario using the rocket equation:

$$m_p = m_f\left(e^{(\Delta v/gI_{sp})} - 1\right) \quad (7)$$

where m_f is the dry mass after the braking burn and I_{sp} is the specific impulse, e.g. equation 17–7 in Wertz and Larson (1999). Assuming a solid rocket motor with $I_{sp} = 250$ s, for a launch $\Delta v = 1000$ m/s, a dry mass estimate of 15 kg (steel casing and motor), and 13.9 kg of RDX, we obtain 14.6 kg of propellant, totaling 43.5 kg. For the IE scenario, with $\Delta v = 1700$ m/s, 16.1 kg of dense inert mass and 15 kg for the motor mass,[1] we obtain 31.1 kg of propellant, total-

[1] This mass is not used in the copper projectile mass estimate for a crater of radius 2 m (Section 2.3), since it encapsulates the propellant volume, giving it a low net density. It is also likely to fracture apart on impact. At any rate, not including this mass makes our estimate conservative.

ing 62.2 kg. Therefore, from a mass perspective, the EE scenario may be advantageous. Finally, we note that for the EE scenario, after a backwards-pointing launch, the projectile's long-axis must be aligned with its velocity vector to ensure penetration. This can be accomplished by building the projectile pre-oriented, and thrusting through its center of mass, provided this imparts minimal post-burn angular rates.

4.2. Sample collector and additional concerns

The capture mechanism may be aerogel or a roll-up fabric collector as proposed by Pieters et al. (1999), depending on the capacity of these materials to absorb many grams of ejected grains. Materials collected at ~2 km/s with aerogel are predicted to have shock pressures lower than 1 GPa (Kitazawa et al., 1999). RDX has a detonation velocity of 8750 m/s, and will have a spike shock pressure of 34 GPa (via equation 2′d in Köhler et al., 2002), but the fraction of material shocked at these values would be limited. Chemical contamination of samples would be minimal, since RDX contains primarily oxygen, nitrogen, and carbon, and could be prepared in a clean environment for the mission. High-speed video cameras on the spacecraft would be useful for imaging the crater event, as would high-resolution multi-band imaging of the crater area. For protecting the spacecraft from debris, we note Stardust carried a Whipple shield designed for 1 cm particles at 6 km/s (Ishiguro et al., 2003).

5. Conclusion

A leading spacecraft loaded with projectiles, equipped either with explosives (~44 kg each) or an inert copper mass (~62 kg each), could produce ejecta curtains with cross sectional densities of 1–10 g/m^2 at heights of 150 m, 4–10 s after impact. A trailing spacecraft could intercept this mass, return to a safe altitude, repeat the process at other sites, and return to Earth. A higher mass could be collected by flying at lower altitudes or increasing the size of the crater. The inert impact excavator scenario could be the simpler approach if oblique impacts can be accommodated. These results are offered to provide scientists and engineers with a sense of the requirements and trades of such a mission.

Acknowledgements

We are most grateful for the helpful comments from two anonymous reviewers.

References

A'Hearn, M.F., Belton, M.J.S., Delamere, W.A., et al. Deep Impact: excavating comet Tempel-1. Science 310, 258–264, 2005.

Anderson, C.E., Orphal, D.L., Franzen, R.R., Walker, J.D. On the hydrodynamic approximation for long-rod penetration. Int. J. Impact Eng. 22, 23–43, 1999a.

Anderson, C.E., Wilbeck, J.S., Elder, J.S. Long-rod penetration into highly oblique, water-filled targets. Int. J. Impact Eng. 23, 1–12, 1999b.

Anderson, J.L.B., Schultz, P.H., Heineck, J.T. Asymmetry of ejecta flow during oblique impacts using three-dimensional particle image velocimetry. J. Geophys. Res. 108, 5094, doi:10.1029/2003JE002075, 2003.

Andrews, R.J. Origin and distribution of ejecta from near-surface laboratory-scale cratering experiments. Report AFW-TR-74-314, Air Force Weapons Laboratory, Kirtland Air Force Base, NM, 1975.

Bence, A.E., Papike, J.J. Pyroxenes as recorders of lunar basalt petrogenesis: chemical trends due to crystal–liquid interaction. Proc. Lunar Sci. Conf. 3rd, 431–469, 1972.

Brownlee, D.E., Flynn, G., Hörz, F., et al. Comet samples returned by the Stardust mission, in: Proc. Lunar Planet. Sci. Conf. 37th, abstract 2286, 2006.

Burgess, R., Turner, G. Laser argon-40–argon-39 age determinations of Luna 24 mare basalts. Meteorit. Planet. Sci. 33, 921–935, 1998.

Cohen, B.A., Snyder, G.A., Hall, C.M., Taylor, L.A., Nazarov, M.A. Argon-40–argon-39 chronology and petrogenesis along the eastern limb of the Moon from Luna 16, 20 and 24 samples. Meteorit. Planet. Sci. 36, 1345–1366, 2001.

Coish, R.A., Taylor, L.A. Mineralogy and petrology of basaltic fragments from the Luna 24 drill core. Mare Crisium: The view from Luna 24, in: Proceedings of the Conference, Houston, TX, December 1–3, 1977. Pergamon Press, New York, pp. 403–417, 1978.

Culler, T.S., Becker, T.A., Muller, R.A., Renne, P.R. Lunar impact history from 40Ar/39Ar dating of glass spherules. Science 287, 1785–1788, 2000.

Delano, J.W. Pristine lunar glasses: criteria, data, and implications. J. Geophys. Res. 91, D201–D213, 1986.

Duke, M.B. Challenges for sample return from the lunar South Pole-Aitken basin, in: Proc. Lunar Planet. Sci. Conf. 34th, abstract 1684, 2003.

Forrestal, M.J., Luk, V.K. Penetration into soil targets. Int. J. Impact Eng. 12, 427–444, 1992.

Gaddis, L.R., Staid, M.I., Tyburczy, J.A., Hawke, B.R., Petro, N.E. Compositional analyses of lunar pyroclastic deposits. Icarus 161, 262–280, 2003.

Garrick-Bethell, I., Zuber, M.T. An indigenous origin for the South Pole-Aitken basin thorium anomaly. Geophys. Res. Lett. 32, L13203, doi:10.1029/2005GL023142, 2005.

Gault, D.E. Impact cratering, in: Greeley, R., Schultz, P.H. (Eds.), A Primer in Lunar Geology. NASA Ames, Moffett Field, pp. 137–175, 1974.

Gault, D.E., Wedekind, J.A. Experimental studies of oblique impact. Proc. Lunar Planet. Sci. Conf. 9th, 3843–3875, 1978.

Hagerty, J.J., Shearer, C.K., Vaniman, D.T. Heat-producing elements in the lunar mantle: insights from ion microprobe analyses of lunar pyroclastic glasses. Geochim. Cosmochim. Acta 70, 3457–3476, 2006a.

Hagerty, J.J., Lawrence, D.J., Hawke, B.R., Vaniman, D.T., Elphic, R.C., Feldman, W.C. Estimating thorium abundances of basalt ponds in South Pole Aitken basin: implications for the composition of the farside lunar mantle, in: Proc. Lunar Sci. Conf. 37th, abstract 1770, 2006b.

Heiken, G., Vaniman, D., French, B.M. Lunar Sourcebook: A User's Guide to the Moon. Cambridge U. Press, Cambridge, England, UK, 736 pp, 1991.

Heiken, G. Petrology of lunar soils. Rev. Geophys. Space. Phys. 13, 567–587, 1975.

Heywood, H. Particle size and shape distribution for lunar fines sample 12057,72. Proc. Lunar Sci. Conf. 2nd, 1989–2001, 1971.

Housen, K.R., Schmidt, R.M., Holsapple, K.A. Crater ejecta scaling laws: fundamental forms based on dimensional analysis. J. Geophys. Res. 88, 2485–2499, 1983.

Ishiguro, M., Kwon, S.M., Sarugaku, Y., et al. Discovery of the dust trail of the Stardust comet sample return mission target: 81P/Wild 2. Astrophys. J. Lett. 589, L101–L104, 2003.

Jolliff, B.L., Haskin, L.A., Korotev, R.L., et al. Scientific expectations from a sample of regolith and rock fragments from the interior of the

South Pole-Aitken basin, in: Proc. Lunar Planet. Sci. Conf. 34th, abstract 1989, 2003.

Kitazawa, Y., Fujiwara, A., Kadono, T., et al. Hypervelocity impact experiments on aerogel dust collector. J. Geophys. Res. 104, 22,035–22,052, 1999.

Köhler, J., Meyer, R., Homburg, A. Explosives, fifth ed VCH Verlagsgesellschaft, Germany, 457 pp, 2002.

Lawrence, D.J., Hawke, B.R., Hagerty, J.J., Elphic, R.C., Feldman, W.C., Prettyman, T.H., Vaniman, D.T. Evidence for a high-Th, evolved lithology on the Moon at Hansteen Alpha. Geophys. Res. Lett. 108, L07201, doi:10.1029/2005GL022022, 2005.

Ma, M.-S., Schmitt, R.A., Taylor, G.J., Warner, R.D., Lange, D.E., Keil, K. Chemistry and petrology of Luna 24 lithic fragments and less than 250-micron soils – constraints on the origin of VLT mare basalts. Mare Crisium: The view from Luna 24; Proceedings of the Conference, Houston, TX, December 1–3, 1977. Pergamon Press, New York, pp. 569–592, 1978.

Melosh, H.J. Impact Cratering. Oxford U. Press, Oxford, 256 pp, 1989.

Nelson, R.W. Low-yield earth-penetrating nuclear weapons. Sci. Global Secur. 10, 1–20, 2002.

Oberbeck, V.R. Laboratory simulation of impact cratering with high explosives. J. Geophys. Res. 76, 5732–6749, 1971.

Pavlis, D.E., Poulose, S.G., McCarthy, J.J. GEODYN operations manuals, Contractor report, SGT Inc., Greenbelt, MD, 2006.

Piekutowski, A.J. Formation of bowl-shaped craters. Proc. Lunar Planet. Sci. Conf. 11th, 2129–2144, 1980.

Pieters, C.M., Calvin, W., Cheng, A., et al. Aladdin: exploration and sample return of Phobos and Deimos, in: Proc. Lunar Planet. Sci. Conf. 30th, abstract 1155, 1999.

Pike, R.J. Apparent depth/apparent diameter relations for lunar craters. Proc. Lunar Sci. Conf. 8th, 3427–3436, 1977.

Shearer, C.K., Borg, L.E. Big returns on small samples: lessons learned from the analysis of small lunar samples and implications for the future scientific exploration of the Moon. Chemie der Erde. Geochemistry 66, 163–185, doi:10.1016/j.chemer.2006.03.002, 2006.

Smith, D.E., Zuber, M.T., Neumann, G.A., Lemoine, F. Topography of the Moon from the Clementine lidar. J. Geophys. Res. 102, 1591–1611, 1997.

Smith, D.E., Zuber, M.T. Measuring the lunar topography with the laser altimeter on LRO. American Geophysical Union Fall Meeting, San Francisco, abstract G53C-02, 2005.

Smith, J.V. Lunar mineralogy: a heavenly detective story, Part I. Am. Miner. 59, 231–243, 1974.

Smith, J.V., Steele, I.M. Lunar mineralogy: a heavenly detective story, Part II. Am. Miner. 61, 1059–1116, 1974.

Steele, I.M., Smith, J.V. Minor elements in lunar olivine as a petrologic indicator. Proc. Lunar Sci. Conf. 6th, 451–467, 1976.

Stöffler, D., Gault, D.E., Wedekind, J., Polkowski, G. Experimental hypervelocity impact into quartz sand: distribution and shock metamorphism of ejecta. J. Geophys. Res. 80, 4062–4077, 1975.

Taylor, G.J., Warner, R.D., Wentworth, S. Keil, K., Sayeed, U., Luna 24 lithologies: petrochemical relationships among lithic fragments, mineral fragments, and glasses. Mare Crisium: The view from Luna 24, in: Proceedings of the Conference, Houston, TX, December 1–3, 1977. Pergamon Press, New York, pp. 303–320, 1978.

Vaniman, D.T., Labotka, T.C., Papike, J.J., Simon, S.B., Laul, J.C. The Apollo 17 drill core: petrologic systematics and identification of a possible Tycho component. Proc. Lunar Sci. Conf. 10th, 1185–1227, 1979.

Vortman, L.J. Ten years of high explosive cratering research at Sandia laboratory. Nucl. Appl. Technol. 7, 269–304, 1969.

Wada, K., Senshu, H., Matsui, T. Numerical simulation of impact cratering on granular material. Icarus 180, 528–545, 2006.

Walker, J.D., Freitas, C.J., Tapley, M.B. Rapid impactor sample return (RISR) mission scenario. Adv. Space Res. 33, 2270–2275, 2004.

Wertz, J.R., Larson, W.J. Space Mission Analysis and Design, third ed Microcosm Press, California, 969 pp, 1999.